6.1 General Observations.

The experimental results presented in this thesis demonstrate that reproducible Argon discharges with substantial quasi-steady driven currents can be produced by external coil structures in a device with conventional toroidal geometry. The driven toroidal current can be maintained for the entire duration of the RF pulse, with no evidence of disruptions.

6.1.1 Driven Toroidal Current.

As seen in Figures 5.8–5.11, the time behaviour of the driven toroidal current is strongly dependent upon the filling gas pressure and the values of the steady applied toroidal and vertical magnetic fields. In these experiments, the external toroidal magnetic field was always applied in a diamagnetic sense with respect to the ΔB_{tor} produced by the driven poloidal current. A number of observations can be made regarding the measurements shown in Figures 5.8–5.11.

(a) There is an optimum value of applied toroidal field for RF current drive. In these exploratory experiments the optimum value of the toroidal field was approximately 480G. It should be mentioned that in some preliminary experiments which are not reported here, substantial toroidal current was driven in the absence of an applied toroidal magnetic field. This fact clearly demonstrates that excitation of plasma waves is not necessary for the current drive mechanism presented in this thesis.

(b) The 'best' current waveforms (i.e. those discharges where the driven toroidal current is largest for the longest length of time), were generally obtained with the lower values of vertical magnetic field.

(c) A current plateau is observed for large values of vertical magnetic field and small values of toroidal magnetic field. DURANCE(1983) has reported similar current

plateaux in early Rotamak experiments using the same Line Generators.

(d) The 'best' driven toroidal current waveforms are not obtained with the plasma located centrally in the minor section of the device. Instead, the B_z probe signal indicates that the centroid of I_{tor} is displaced towards the outer wall of the vacuum vessel.

(e) The driven toroidal current can be centred in the minor section of the vacuum vessel by increasing the strength of the applied vertical magnetic field. However, with a large applied vertical field, increases in the vertical field strength were found to progressively reduce the duration of the driven toroidal current.

6.1.2 Poloidal Magnetic Flux Contours

The ability to construct meaningful poloidal magnetic flux contours from a large number of separate plasma shots performed under the same experimental conditions is testimony to the reproducibility of the Rythmac discharges. Poloidal flux contour plots have been obtained in discharges where the external toroidal magnetic field is either diamagnetic or paramagnetic with respect to the toroidal field produced by the driven poloidal current. Discharges with closed poloidal flux contours can be produced in the presence of a diamagnetic steady external toroidal magnetic field.

In discharges where the external toroidal field was paramagnetic with respect to the field produced by the driven poloidal current (Figure 5.23), no closed poloidal flux contours were observed. In this case, confinement of the plasma in the minor radial direction is expected to be worse than for the corresponding diamagnetic configuration. The plasma is expected to lean against the vacuum vessel wall to a larger degree (wall confinement).

In the paramagnetic configuration of Data Set 3, the driven toroidal plasma current was found to be larger for longer than in the corresponding diamagnetic configuration (Data Set 2). This observation may be explained by the fact that in the

paramagnetic case, the plasma is expected to lie closer to the external RF windings, where the amplitude of the applied RF field is larger.

6.2 Derivation of Additional Plasma Parameters

In this section, we attempt a quantitative comparison between $m = 1$ double-helix current drive theory and experiments. The theory presented in Chapter 2 is used to model the double-helix current drive experiments described in Section 5.5.1 of Chapter 5. The results of these experiments have been presented in Table 5.3.

The dimensionless quantities λ and γ_ω introduced in Chapter 2 were used as free parameters in the theory. The values of λ and γ_ω were systematically varied in order to fit the experimentally measured quasi-steady toroidal and poloidal plasma currents. Recalling the definitions in Chapter 2, we have:

$$\lambda = \frac{a}{\delta} = a\left(\frac{2m_e\nu_{ei}}{\mu_0\omega n_e e^2}\right)^{-\frac{1}{2}} \tag{6.1}$$

$$\gamma_\omega = \frac{\omega_{ce}}{\nu_{ei}} = \frac{eB_\omega}{m_e\nu_{ei}} \tag{6.2}$$

Since the amplitude, B_ω, and the angular frequency, ω, of the vacuum RF magnetic field are known, the values of λ and γ_ω obtained from the fitting process can be used to yield estimates of the average electron number density, n_e, and the average electron-ion collision frequency, ν_{ei}, in the plasma. From equation (6.1) and equation (6.2) we find:

$$n_e = \frac{2\lambda^2}{\gamma_\omega}\frac{B_\omega}{\mu_0 e\omega a^2} \tag{6.3}$$

$$\nu_{ei} = \frac{eB_\omega}{m_e\gamma_\omega} \tag{6.4}$$

In Table 6.1, we present the estimated values of n_e and ν_{ei} obtained by fitting the experimentally observed plasma currents and the steady external axial (toroidal) magnetic field, at each line generator charging voltage listed in Table 5.3. In the theory,

the value of the external axial magnetic field was taken to be the value of the vacuum toroidal magnetic field at the centre of the minor section ($B_{0z}^{ext} = B_{\phi vac}(R_0, 0) =$ 128G). The filling gas in these experiments was Argon at 1mTorr.

The average electron number density obtained from the theory can be used to estimate an effective ion charge number, Z_{eff}, where:

$$n_e = Z_{eff}\, n_0 \tag{6.5}$$

Here n_0 denotes the initial filling density of Argon atoms. In the present calculations we take $n_0 = 3.5 \times 10^{19}\text{atoms/m}^3$ which corresponds to an initial filling pressure of 1.0mTorr. On the average, all the Argon atoms which are initially present are assumed to provide an equal number of electrons, so that it is possible to produce discharges with whole or fractional values of Z_{eff}. A more accurate determination of Z_{eff} could be obtained by experimental measurement of the plasma electron and ion densities.

Dr. S. Ortolani of the University of Padua (Private Communication) has calculated the effective ion charge number, Z_{eff}, for Argon at various electron temperatures, T_e, using a corona model. The results of this calculation have been replotted in Figure 6.1 and have been used to obtain the estimated values of T_e given in Table 6.1.

Following KNIGHT(1988), the average electron-ion collision frequency in the plasma can be estimated from the values of n_e, Z_{eff} and T_e given in Table 6.1. The Spitzer resistivity (from CHEN(1984)) for $Z_{eff} \simeq 1$ is,

$$\eta_s = 5.2 \times 10^{-5} \frac{Z_{eff} \ln \Lambda}{T_e^{3/2}[\text{eV}]} \quad \Omega\text{m} \tag{6.6}$$

where the Coulomb cutoff parameter, Λ, given by TANENBAUM(1967) is,

$$\Lambda = 1.54 \times 10^{13} \frac{T_e^{3/2}[\text{eV}]}{n_e^{1/2}[\text{m}^{-3}]} \tag{6.7}$$

Equating the Spitzer resistivity to the scalar resistivity,

$$\eta = \frac{m_e \nu_{ei}}{n_e e^2} \tag{6.8}$$

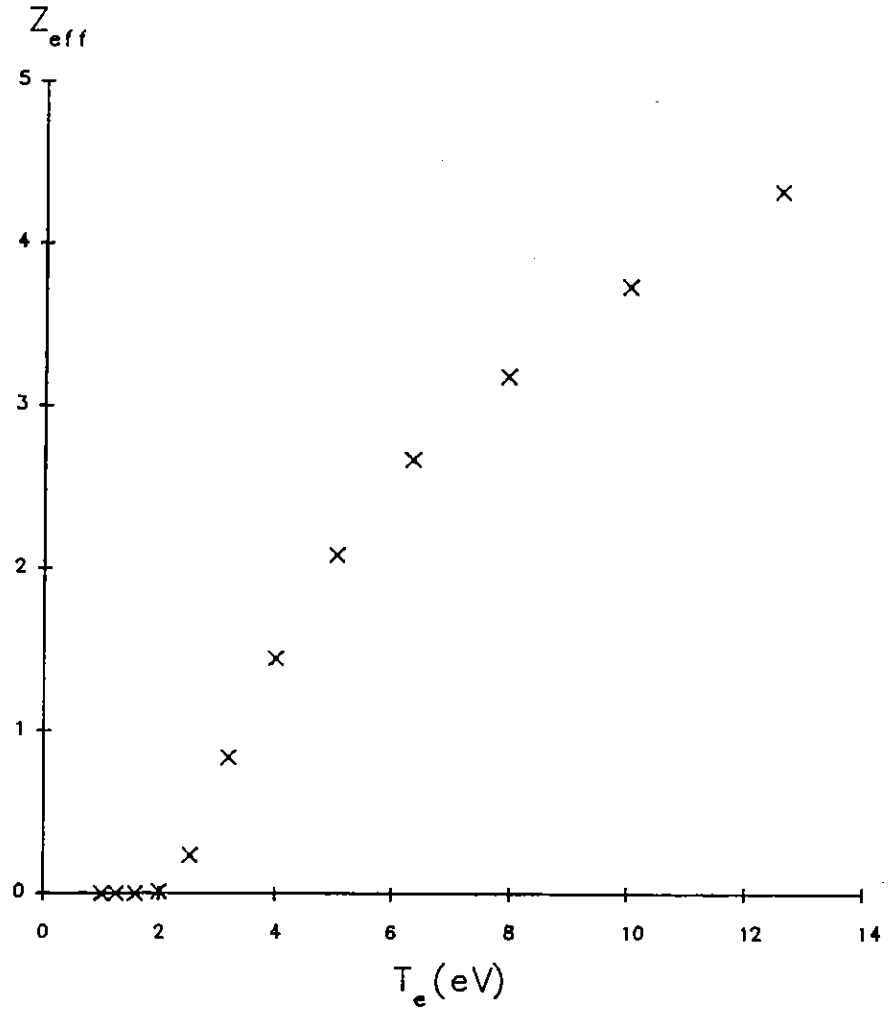

Figure 6.1 Plot of the effective ion charge number Z_{eff} for Argon as a function of electron temperature T_e. The calculations were performed by Dr. S. Ortolani of the University of Padua (Private Communication).

we find that:

$$\nu_{ei} \simeq 5.2 \times 10^{-5} \frac{n_e e^2 Z_{eff} \ln \Lambda}{m_e T_e^{3/2}} \quad \mathrm{s}^{-1} \tag{6.9}$$

where T_e is in electron volts and n_e is in electrons/m^{-3}. The values of ν_{ei} obtained using equation (6.9) are shown in parentheses in Table 6.1. The values of ν_{ei} found from the theory and from the Spitzer resistivity agree very well at the lowest line generator charging voltage and differ by less than a factor of two at the highest charging voltage.

In Figure 6.2, we plot the estimated values of the electron density, electron temperature and electron-ion collision frequency (using both methods), which are obtained for each line generator charging voltage. The values of the plasma parameters are consistent with the types of Argon discharges produced in closely related Rotamak devices. DURANCE(1983) used the same line generators to produce a Rotamak configuration in Argon with an average electron number density of $n_e \simeq 5 \times 10^{19} \mathrm{m}^{-3}$ and an estimated (but not measured) electron temperature of the order of 5eV.

6.3 Major-Radial Force Balance

In this section we estimate the strength of the various forces along the major-radial direction in the Rythmac-1 device at the time of peak driven toroidal and poloidal plasma current (approximately 15μs after the start of the discharge).

We find that the force arising from the interaction of the quasi-steady driven poloidal current with the steady toroidal magnetic field plays an important role in the equilibrium. It was the desire to control the strength of this particular force (by reducing the magnitude of the driven poloidal current) that lead to the development of the 'helical-mesh' antenna described earlier.

An external vertical magnetic field is applied in order to balance the radially outward forces and achieve radial equilibrium. The vertical field is also necessary to achieve equilibrium in the vertical direction, although this will not be discussed here.

Plasma Parameter	Line Generator Charging Voltage (kV)				
	20	22	24	26	28
λ	8.37	8.50	9.41	8.48	8.22
γ_ω	44.6	45.9	42.1	22.6	18.3
$\bar{B}_\omega$ (G)	55	62	70	78	83
B_{oz}^{ext} (G)	128.1	128.3	125.0	127.5	127.7
I_{tor} (A)	423 (420)	482 (480)	741 (600)	786 (750)	933 (910)
I_{pol} (A/m)	5965 (6000)	6730 (6800)	9595 (9500)	15670 (15700)	18660 (18700)
$n_e(\times 10^{19}\mathrm{m}^{-3})$	1.8	2.0	2.7	4.3	5.2
Z_{eff}	0.52	0.57	0.80	1.24	1.50
T_e (eV)	2.8	2.9	3.1	3.7	4.1
$\nu_{ei}(\times 10^7\mathrm{Hz})$	2.4 (2.8)	2.5 (3.3)	2.9 (5.7)	5.5 (11.1)	7.1 (13.8)

Table 6.1: Estimates of plasma parameters extracted from theory by fitting the experimentally observed peak quasi-steady driven plasma currents (given in parentheses) and steady externally applied 'axial' magnetic field ($B_{0z}^{ext} \simeq B_{\phi vac}(R_0, 0) = 128\mathrm{G}$). The values of electron-ion collision frequency in parentheses are calculated from Z_{eff} and T_e using the Spitzer resistivity (Equation (6.9)).

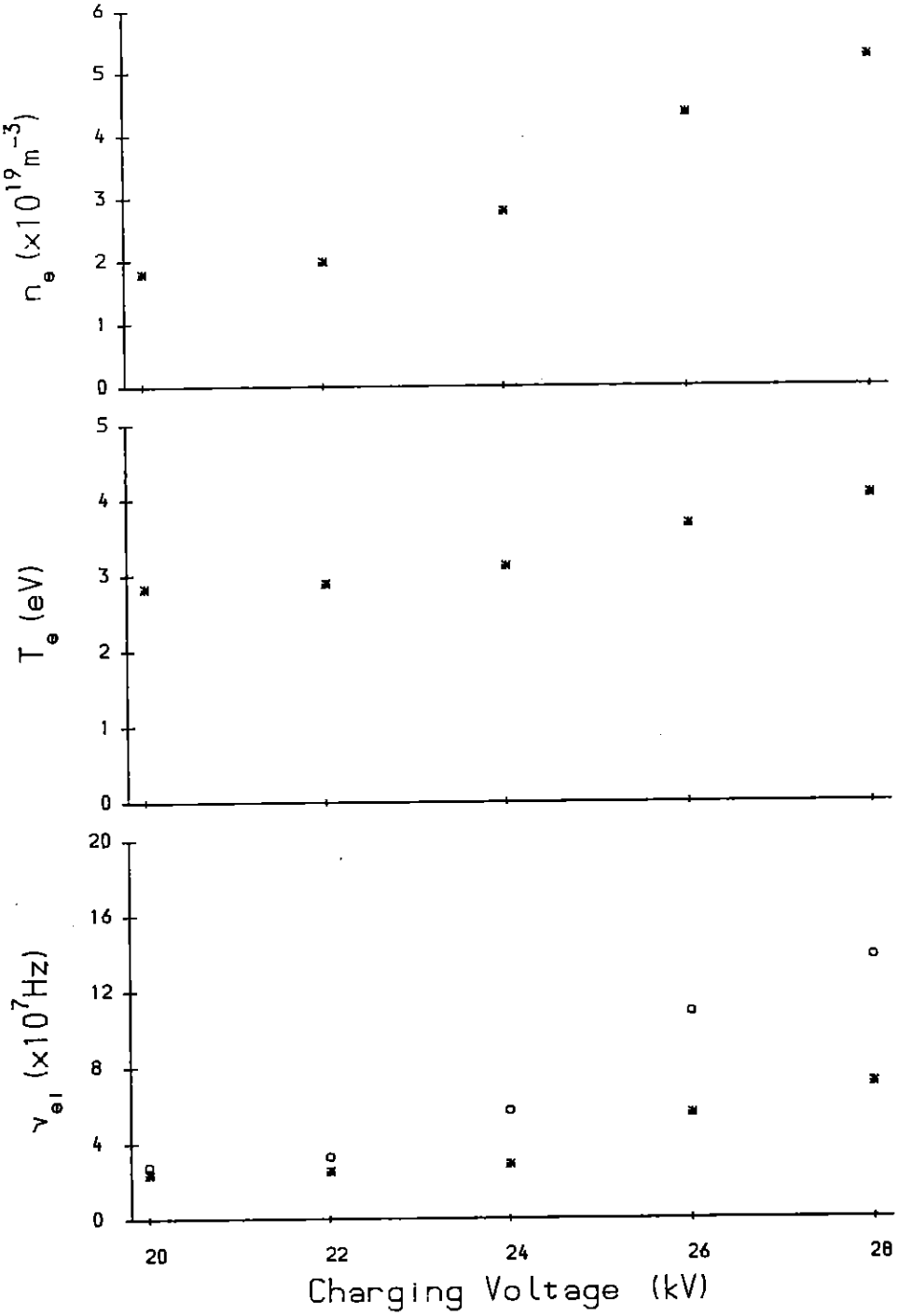

Figure 6.2 Plots of the plasma parameter estimates given in Table 6.1, which were obtained from a quantitative comparison between theory and experiment. The plots show the dependence on the line generator charging voltage of (a) electron number density, (b) electron temperature and (c) electron-ion collision frequency in the plasma. The circles indicate values of electron-ion collision frequency obtained from the Spitzer resistivity (equation (6.9)).

The appropriate strength of the applied vertical field was chosen to be the value for which the largest quasi-steady toroidal current was driven for the longest length of time (i.e. B_v was chosen to maximise $\int I_{tor} dt$). This choice of B_v did not ensure that the plasma was centred in the minor section. Instead, the plasma was found to be displaced towards the outer wall of the vacuum vessel.

In a steady state tokamak-like plasma, the outward forces along the major radius arise from (a) the plasma pressure (b) the interaction of the toroidal current (J_ϕ) with the poloidal magnetic field (B_θ), and (c) the interaction of the poloidal current (J_θ) with the toroidal magnetic field (B_ϕ). The magnitudes of each force (and the confining force provided by the vertical field) are calculated for a typical discharge in the Rythmac-1 device using expressions given by BATEMAN(1978). The experimental conditions under which data for poloidal flux contour Data Set 6 (Table 5.4) was collected are taken to be representative of discharges in Rythmac-1. The design and operating parameters for Rythmac-1, and the values of plasma parameters obtained for Data Set 6 are summarised for convenience in Table 6.2.

Plasma pressure

The magnitude of the outward force due to the plasma pressure, distributed around the whole of the torus is, from BATEMAN(1978):

$$F_p = 2\pi \int d\boldsymbol{S} \cdot \hat{\phi}\, p(\psi) \tag{6.10}$$

Where the pressure is specified in terms of the stream function, ψ, and $\int d\boldsymbol{S} \cdot \hat{\phi}$ denotes integration over the minor section of the torus. In order to estimate the size of F_p we assume that the plasma pressure is constant over the minor section and the ions are cold ($T_i \ll T_e$). Equation (6.10) then reduces to,

$$F_p \simeq 2\pi^2 a^2 n_e k T_e \tag{6.11}$$

Rythmac-1 parameters		plasma parameters	
major radius	$R_0 = 25\text{cm}$		
minor radius	$a = 5\text{cm}$	Argon filling pressure	$p = 1.0\text{mTorr}$
line generator voltage	$V_0 = 28\text{kV}$	peak toroidal current	$I_{tor} = 1.2\text{kA}$
RF frequency	$f = 330\text{kHz}$	change in toroidal field*	$\Delta B_{tor} = 230\text{G}$
inverse pitch of RF coils	$\kappa = 0.8$	peak poloidal current	$I_{pol} = 18.3\text{kA/m}$
vacuum RF field strength*	$B_\omega \simeq 80\text{G}$	est. electron density	$n_e \simeq 5 \times 10^{19}\text{m}^{-3}$
external toroidal field*	$B_{tor} = 160\text{G}$	est. electron temp.	$T_e \simeq 4\text{eV}$
external vertical field*	$B_v = 36\text{G}$		

*Magnetic field values are measured at the centre of the minor section ($r = R_0, z = 0$).

Table 6.2: Summary of Rythmac-1 device parameters and experimental plasma parameters for typical discharge conditions described by Data Set 6 (see Table 5.4).

which on substituting numerical values from Table 6.2 yields:

$$F_p \simeq 2.3\text{N}$$

Toroidal current: $J_\phi \times B_\theta$

BATEMAN(1978) has calculated the net outward force due to the interaction of the steady toroidal plasma current with the poloidal magnetic field to be:

$$F_{B_\theta} = \frac{1}{2}\mu_0 I_\phi^2 \left[\ln\frac{8R_0}{a} - 1 + \frac{\ell_i}{2}\right] \tag{6.12}$$

where $\ell_i \geq \frac{1}{2}$ for uniform or mildly peaked current distributions. From equation (6.12), we find that numerically,

$$F_{B_\theta} = 2.9\text{N}$$

Poloidal current: $J_\theta \times B_\phi$

Again from BATEMAN(1978), the net outward force due to the interaction of the driven poloidal current with the steady toroidal magnetic field is:

$$F_{B_\phi} = 2\pi \int d\boldsymbol{S} \cdot \hat{\boldsymbol{\phi}} \frac{1}{2\mu_0}(B^2_{\phi vac} - B^2_\phi) \tag{6.13}$$

The vacuum toroidal magnetic field is given by:

$$B_{\phi vac} = B^{ext}_\phi \frac{R_0}{R} \tag{6.14}$$

where $B^{ext}_\phi = 160\text{G}$ and R is the major radial coordinate. A good approximation to the integral on the righthand side of equation (6.13) can be obtained analytically by using the form of the toroidal magnetic field in the presence of the plasma obtained from equation (2.98). i.e.

$$B_\phi = \left[B^{ext}_\phi + \frac{1 - \mathrm{x}^2}{2 + \kappa^2} \mu_0 n e \omega a^2 \right] \frac{R_0}{R} \tag{6.15}$$

The multiplicative factor of R_0/R has been included to allow for toroidicity. Equation (6.15) can be rewritten as:

$$B_\phi = \left[B^{ext}_\phi + (1 - \mathrm{x}^2) \Delta B_\phi \right] \frac{R_0}{R} \tag{6.16}$$

where $\mathrm{x} = r/a$ is the normalised minor radial coordinate and $\Delta B_\phi = -230\text{G}$ is chosen to give the experimentally measured change in the steady toroidal magnetic field at $(R = R_0, z = 0)$. Analytic integration of the righthand side of equation (6.13) over the minor section of the vacuum vessel now yields the expression,

$$F_{B_\phi} = -\frac{\pi^2 a^2}{\mu_0} \Delta B_\phi \left[B^{ext}_\phi + \frac{1}{4} \Delta B_\phi \right] \tag{6.17}$$

from which we find that:

$$F_{B_\phi} = 4.6\text{N}$$

Outward		Inward	
Plasma pressure	+2.3N	Vertical field	−6.8N
$J_\phi \times B_\theta$	+2.9N		
$J_\theta \times B_\phi$	+4.6N		
TOTAL	+9.8N	TOTAL	−6.8N

Table 6.3: Summary of major-radial forces for a typical Rythmac-1 discharge (Data Set 6, $t \simeq 15\mu$s).

Vertical field

The inward force along the major-radial direction due to the interaction of the applied vertical magnetic field with the driven toroidal current is given by:

$$F_{B_v} = -2\pi R_0 B_v I_\phi \tag{6.18}$$

which for the Rythmac-1 discharge under consideration has a numerical value of,

$$F_{B_v} = -6.8\text{N}$$

The magnitudes of the various forces in the major-radial direction (in Newtons) are summarised in Table 6.3. It is clear that the outward forces along the major radius are not completely balanced by the vertical field alone. However, the fact that discharges performed under these conditions were highly reproducible suggests that equilibrium must be achieved with the aid of an additional confining force. From Table 6.3, the magnitude of this additional confining force must be approximately 3N.

The extra confining force is believed to arise partly from the RF magnetic pressure, $\langle \tilde{b}^2 \rangle / 2\mu_0$, but mainly from image currents induced in the vertical field coils and the RF windings. A simple estimate of the confining force due to the RF pressure shows that this force is not significant unless the plasma column is very close to the external

RF conductors, which was not the case in the experiments. The bulk of the additional confining force is expected to arise from image currents which are driven by the loop voltage (Figure 4.8). The loop voltage is produced by the changing poloidal magnetic flux associated with the rapidly rising driven toroidal current.

From an inspection of Figure 3.8 (vertical field coil geometry) we would expect the coupling between the driven toroidal current and the vertical field coils to be relatively strong. Hence, on the short timescale of the experiments, the external coils are expected to act like a conducting shell surrounding the plasma. The magnitude of image currents in the vertical field coils necessary to produce a confining force of 3N can be calculated from equation (6.18) using the Rythmac-1 vertical field coil calibration given in Table 3.1 (0.161 G/A). The maximum image current required is found to be $\sim$ 100A. Image currents of this magnitude could have been present in the experiments.

The presence of image currents induced in the vertical field coils will tend to mask the effect of moderate changes in the vertical field strength, which could account for the lack of significant differences in the poloidal flux contour plots presented in Section 5.7.3.6. The effect of image currents could be reduced by employing a vertical field coil geometry suggested by BELLAN(Private communication,1987) in which the linkage of poloidal flux associated with the driven toroidal current is minimised. However, this could prove to be detrimental in view of the confining effect which the image currents produce.

6.4 Summary and Conclusions

The results of this work have demonstrated both experimentally and theoretically, that the $\langle \tilde{j} \times \tilde{b} \rangle$ current drive technique can be used to drive substantial toroidal and poloidal current in a device with conventional toroidal geometry.

The plasma/field configurations produced in the experiments were very repro-

ducible. The relatively short duration of the RF sources ($\sim 50\mu s$) makes this result even more encouraging, since the discharges were not maintained for very much longer than the duration of the initial 'start-up' phase. Transient behaviour associated with the initial rise of the driven currents (e.g. loop voltage and negative toroidal current density) was evident for the bulk of each plasma shot.

6.5 Future Work

Future experimental work will concentrate on extending the duration of the applied RF pulse well beyond the 'start-up' phase. The medium power ($\sim$ 30kW per phase), long duration (40ms) RF amplifiers used in recent Rotamak experiments at Flinders University [KIROLOUS (1986)] have been used for preliminary (unpublished) long duration Rythmac studies. Construction of high power (400kW per phase), long duration (40ms) RF amplifiers which is currently in progress, is expected to increase the level of available RF power from $\sim$ 60kW to approximately 800kW.

Future work should include experimental measurements of the electron density and temperature distributions in long duration Rythmac discharges. The experimental results could be compared with theoretical estimates to give a much better indication of the validity of the simple $m = 1$ double-helix current drive theory.

The helical mesh antenna appears to overcome the potential difficulties which may arise from the presence of the large poloidal current in $m = 1$ double-helix current drive experiments. Further experimental work in this area is warranted. A theoretical description of helical mesh current drive was beyond the scope of the present work. However, despite the apparent complexity of the problem, this analysis should be attempted in the future.

A considerable amount of theoretical work remains to be done, before a full understanding of $m = 1$ double-helix current drive is possible. At the expense of increasing complexity, the theory presented in Chapter 2 could be improved by including the

effects of ion motion (finite ion temperature) and realistic (non-uniform) density profiles. The influence of higher harmonics of the applied RF field (due to the discrete nature of the external RF coils) could also be investigated.

It must be remembered that the underlying physical model is based on an infinitely long straight plasma cylinder and as such does not include toroidal effects such as the $1/r$ dependence of the applied toroidal field. To satisfactorily include the effects of toroidicity would require solving the appropriate current drive equations in toroidal geometry.